Tunable six-band miniaturised metamaterial absorber for IoT and THz imaging applications

BALU ASHVANTH[ORCID]* and SELVI KANIMOZHI

Department of ECE, Sri Venkateswara College of Engineering, Sriperumbudur 602 117, India
*Corresponding author. E-mail: ashvanthb@svce.ac.in

Abstract. A novel metamaterial absorber with multiband characteristics is proposed to solve the limited bandwidth problem of the internet of things (IoT) backhaul network. The designed tunable absorber has six L-shaped stubs with graphene at the edges to realise six absorption bands of 0.5, 0.78, 1, 1.2, 1.55 and 1.9 THz. The absorption bands are individually tunable by varying the Fermi level of graphene by controlling the electrostatic gating. Hence, tunable absorption characteristics are provided in the optical regime. The absorber is made of polyimide substrate having a unit cell of $0.13\lambda_0 \times 0.13\lambda_0$ dimension, which is smaller than similar kinds of substrates described in the literature. The simulation result shows a better absorption coefficient value of 0.9 over most of the operating bands. The influence of material on the absorption peak is analysed by using different types of conductor and dielectric materials. The designed absorber is a perfect candidate to overcome bandwidth issues in IoT backhaul networks and is also suitable for emerging terahertz applications.

Keywords. Multiband absorber; internet of things; terahertz; graphene; tunable absorber.

PACS Nos 42.79.−e; 42.79.Sz; 42.81.Pa; 81.05.ue

1. Introduction

Internet of things (IoT) is an interconnection of computing devices and objects. They can process or transfer data over the internet by using software, sensors, or other technologies without requiring any human intervention. As IoT devices work autonomously, it is essential to be wireless with accurate sensing capability. The IoT backhaul networks are responsible for transferring data back and forth between IoT devices and the internet. The limited backhaul bandwidth offered by WiFi and licensing issues of the cellular network (LTE, 5G) result in extraneous packets that are discarded at the IoT gateway when it gets overloaded. Establishing optical links across the backhaul network seems to be a perfect solution due to its higher bandwidth and increased reliability. A perfectly designed metamaterial can be a good absorber of light and hence can act as a sensor as demonstrated in [1,2]. The metamaterial absorber-equipped IoT devices have good sensing ability which when merged with optical IoT backhaul network results in increased efficiency and throughput. A tunable single-band metamaterial-based absorber is presented in [3]. The resonance is achieved with the

spacer cavity formed by the metal/strontium titanate (STO)/photoresist metal layers. As the STO layer is sensitive to temperature, the absorption peak can be controlled by changing the measured temperature.

Saadeldin *et al* [4] proposed a design that has a narrow resonant peak with a high absorptivity of 0.99 at 2.249 THz. This makes the metamaterial highly sensitive to the refractive index of the surrounding medium at fixed analytic thickness and hence suitable for biomedical applications. In [5,6], an equivalent circuit model is used to design and analyse a graphene-based metamaterial absorber. The effect of chemical potential of the graphene layer on the absorption frequency is demonstrated for realising tuning over the operating frequency. However, multiple layers are utilised in all these works, which bring structure complexity and make the fabrication difficult. The effects of patterned arrays of one-dimensional or two-dimensional subwavelength graphene elements and sandwiching of graphene layer between aluminium oxide strips and polymethyl methacrylate slab, on the absorption performance of the metamaterial is analysed in [7–9]. However, only dual absorption bands are obtained with this multilayer patterned graphene structure. Broadband

switchable metamaterial absorbers are investigated in [10–14]. Different techniques are used to achieve this switchable response which include using thermally controllable vanadium dioxide (VO$_2$), randomly initialised hill climbing (RHC) algorithm for deciding patch shape, graphene stacks, photoresistive material combined with a heavily doped SiO$_2$ layer. However, these methods complicate the fabrication process and result in high costs. A reconfigurable absorber reported in [15] uses a combination of organic material in crystal form with gold disks. Here, the absorption frequency is reconfigured by selective switching of this organic material through biasing of gold disks. However, this absorber can be fabricated based on wet chemistry for protein or other organic materials. To overcome the challenges in ferrite-based absorbers, a catenary model is used in [16] to design a broadband absorber with ultralow density, which could be useful for applications in aviation and space fields. The plane waves falling on subwavelength-based metasurfaces with periodic slits [17] give a special kind of wave, termed as metasurface wave (M-wave), possessing many interesting properties. Effective methods to realise tunable digital M-waves are realised and dynamic beam-steering is achieved which finds potential applications in the optical phased array (OPA). The metal-organic framework (MOF) derived magnetic/dielectric synergy Ni@C composites with unique nano–microstructure in [18] was designed to be lightweight, wideband and highly efficient microwave absorber materials with a wide bandwidth of 4.7 GHz. A tunable metamaterial absorber for sensing-based IoT applications is proposed in this paper. The designed absorber realises six bands (0.5, 0.78, 1, 1.2, 1.65 and 1.9 THz) between 0.1 THz and 2 THz. Wider spectrum coverage through tuning is achieved by shifting the Fermi level of graphene through proper biasing. Individual tuning of every absorption band is illustrated with simulation results.

The paper is organised as follows: Section 2 describes the design and development of metamaterial absorbers. The formation and control of the absorption band are demonstrated in §3. The tuning process involved in every absorption band is explained in §4 with the necessary simulation results. Various steps involved in designing and fabricating the metamaterial absorber is also illustrated in §4. Section 5 provides the conclusive remarks of this research work.

2. Unit cell design

Figure 1 shows the proposed absorber unit cell. It consists of two copper layers separated by a polyimide dielectric having a refractive index of 3.5. The whole
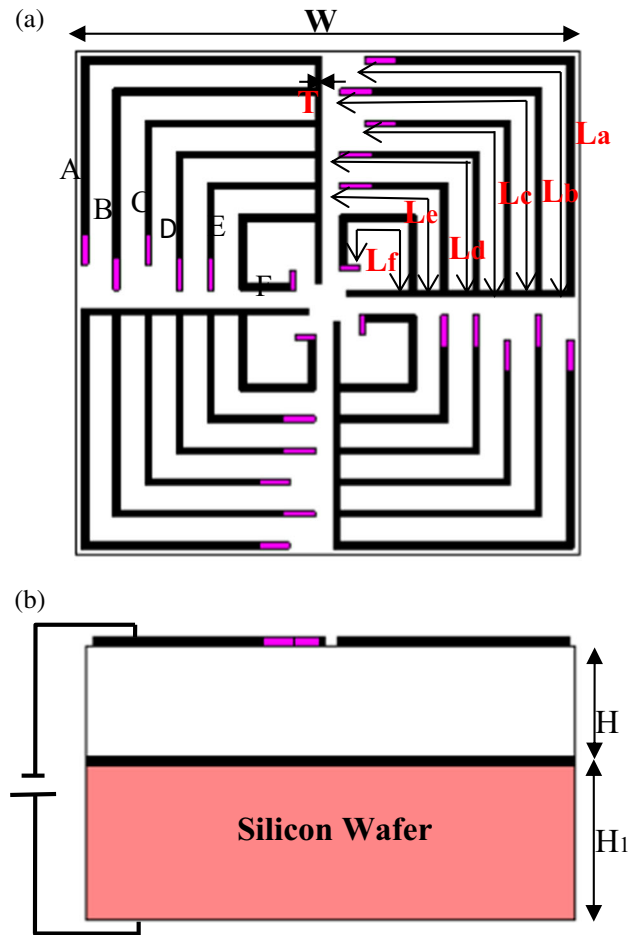

Figure 1. Absorber unit cell. (**a**) Top view and (**b**) side view. Pink colour stands for graphene and black colour stands for copper.

structure is backed by a silicon wafer for providing physical stability to the designed absorber. The unit cell is having a dimension of $80 \times 80\,\mu$m with a dielectric thickness of $H = 18\,\mu$m and silicon wafer height of $H_1 = 50\,\mu$m. Each quadrant of the absorber unit cell is having a common line to which six different sizes of L-shaped stubs A, B, C, D, E, F with dimensions La = 68 μm, Lb = 62 μm, Lc = 48 μm, Ld = 42 μm, Le = 32 μm, Lf = 30 μm, T = 1 μm are connected to provide six absorption bands between 0.1 THz and 2 THz. At the end of each stub, graphene is attached for tuning its corresponding band by applying a bias voltage. The centre connecting point of the patch is etched away to realise six absorption bands with equal spacing having a high absorption coefficient value. The thickness of each copper layer is 0.5μm.

3. Simulation result

looseness-1The stubs A, B, C, D, E, F control the absorption bands 0.5, 0.78, 1, 1.2, 1.55 and 1.9 THz
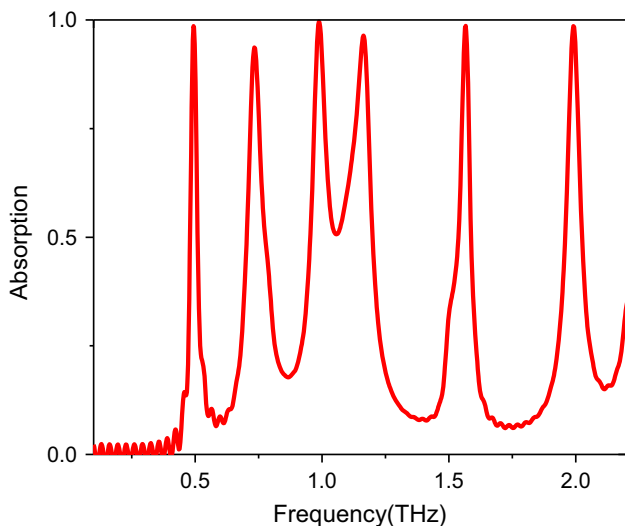
Figure 2. Calculated absorption peaks of the proposed absorber.

respectively which are well illustrated in figure 2. By varying the length of each stub, the corresponding band position is shifted so that most of the frequencies across the operating bandwidth (0.1–2 THz) are covered. As it is not possible to vary the stub length physically, voltage controllable graphene is included at the terminal of every stub. By varying the chemical potential of graphene, its Fermi level changes resulted in the tuning of absorption bands. The schematic diagram of the gate voltage operating graphene Fermi level is shown in figure 1b. Graphene does not have the property of metal but the loss associated with graphene is less than noble metal. Hence, graphene is a perfect candidate to be used in the THz regime. Since transmission of the incident wave through the structure is completely blocked by the metallic ground plane, absorption coefficient A can be calculated as

$$A = 1 - |S_{11}|^2 - |S_{21}|^2 = 1 - |S_{11}|^2, \qquad (1)$$

where A is the absorption coefficient, S_{11} is the reflection coefficient and S_{12} is the transmission coefficient. The dimension of an absorber is optimised in such a way that the peak absorption coefficient value should be around 0.9 for most of the bands as depicted in figure 2. This absorber is designed and simulated with CST microwave studio software.

4. Tuning analysis

Electrostatic bias voltage is used to control the chemical potential of graphenes, which in turn brings variation in its conductivity. The surface conductivity of graphene is determined by

$$f_d = \frac{1}{1 + e^{(\varepsilon - \mu_c)/K_B T}}, \qquad (2)$$

where f_d is the Fermi–Dirac distribution function, ε is the permittivity of graphene, μ_c is the conductivity of graphene corresponding to its chemical potential, K_B is the Boltzmann constant, T is the temperature. The Fermi level of graphene is exponentially related to its conductivity (chemical potential) as illustrated by eq. (2). It has been observed that the conductivity of graphene increases with the increase in the applied bias voltage. This property serves as a simple tuning mechanism based on electrostatic gating. The centre resonance frequency of the sixth band shows an obvious shift from 1.9 to 2.3 THz when increasing the chemical potential of the F stub graphene from 0 to 1 eV as depicted in figure 3a, whereas the fifth band centre frequency shifts from 1.55 to 1.74 THz while increasing the chemical potential of the E stub graphene from 0 to 1.5 eV as shown in figure 3b. Similarly, the remaining four absorption bands are controlled by varying the graphene potential of their respective stubs. The conductivity of graphene depends on the relaxation time. As stub length increases, its associated graphene length should be increased to accomplish maximum tuning. However, in the proposed absorber, due to the size limitation/miniaturisation, the graphene length is kept constant for all the stubs. Thus, the lower absorption bands, because of larger stubs, realise lesser tuning range than the higher bands. Even with this graphene length at A stub, the maximum tuning can be attained by raising the graphene potential to above 5 eV. However, for uniformly analysing the tuning characteristics over all the operating bands, a similar voltage range (0.5–1.5 eV) is chosen for all the six operating bands as indicated by figures 3a–3f.

To understand the performance of the proposed absorber, the surface current distributions are depicted in figure 4. The surface current distribution is analysed at 1.55 and 1.9 THz frequencies corresponding to the centre frequency of the fifth and sixth absorption bands respectively. The absorption peaks at 1.55 and 1.9 THz are due to the fifth and sixth L stubs in each quadrant of the absorber. Hence maximum current exists across them as shown in figures 4a and 4b.
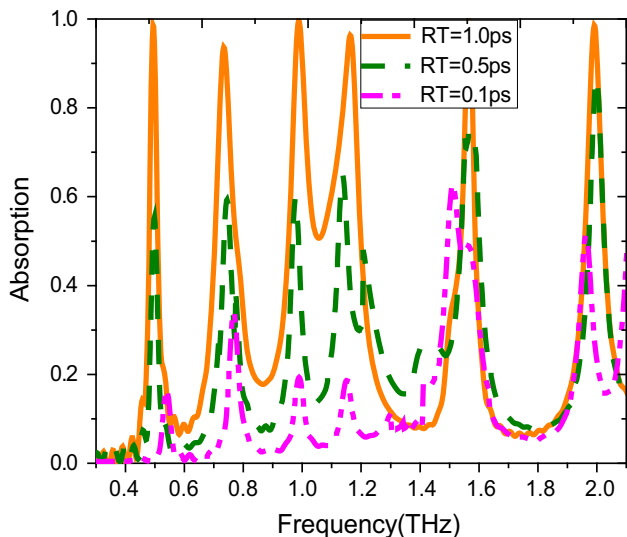
Figure 5 shows the absorption spectra for different relaxation times (RT) of graphene. It can be seen that as RT increases, the amplitude of the absorption peak gradually enhances, while the location of the absorption peak remains almost unchanged. The dependence of the absorption spectra on various materials of the absorber is investigated with graphs shown in figure 6. By using different conducting materials, namely copper (Cu), silver (Ag), gold (Au) for patch and ground plane of the absorber has a negligible effect on the absorption
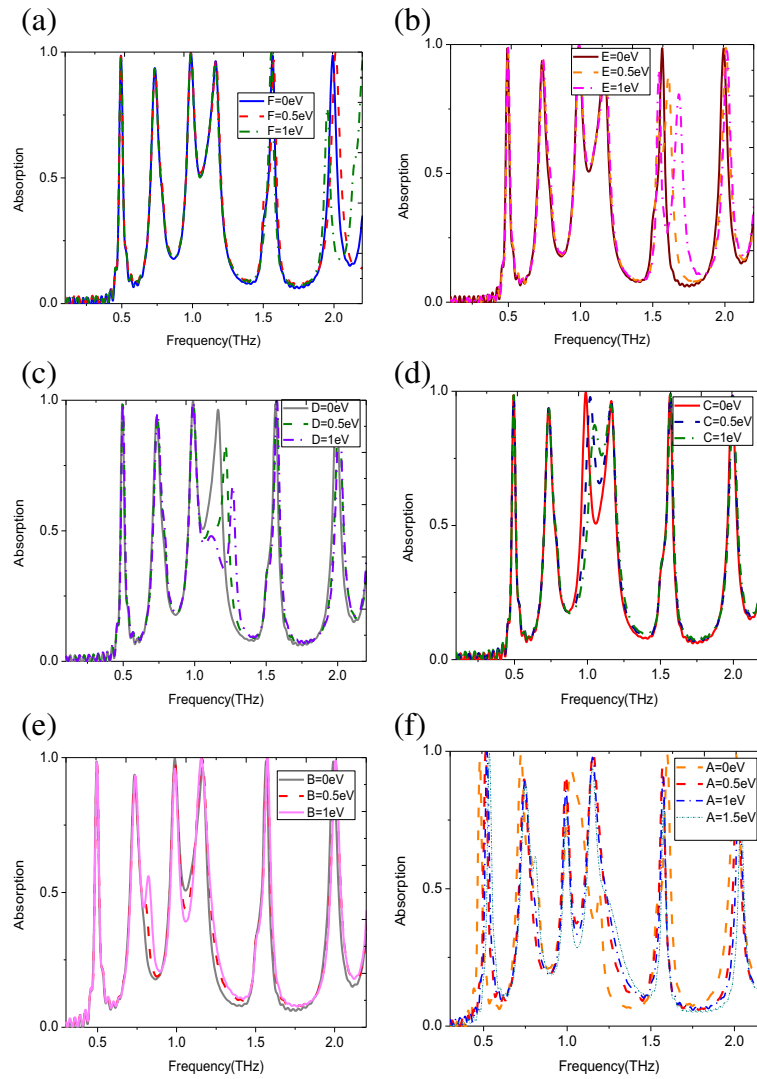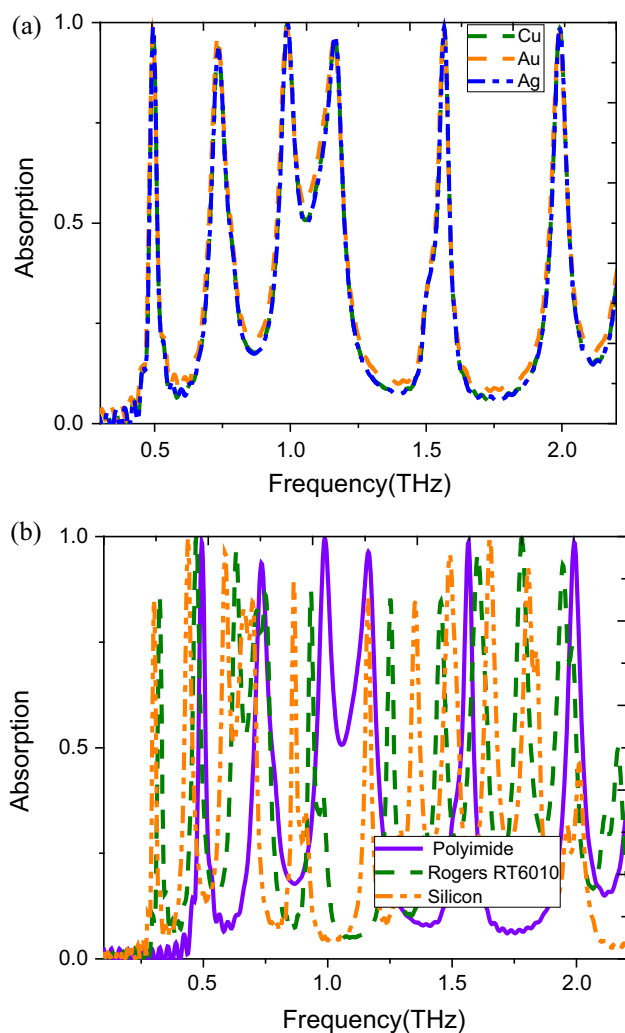
Figure 3. Control of absorption band by using the corresponding L stub graphene potential. (**a**) F stub, (**b**) E stub, (**c**) D stub, (**d**) C stub, (**e**) B stub and (**f**) A stub.
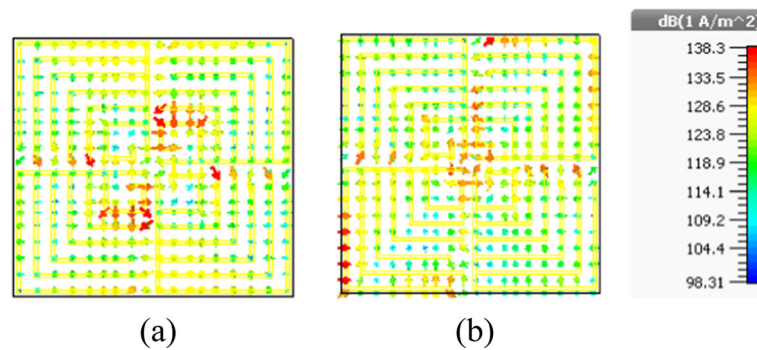
Figure 4. Surface current distributions at (**a**) 1.55 THz and (**b**) 1.9 THz.

Figure 5. Absorption spectra for different relaxation times.

Figure 6. Calculated absorption bands for different (**a**) conductors and (**b**) dielectrics.

rate as shown in figure 6a. From figure 6 it is observed that the proposed absorber realises six bands of absorption with their respective centre frequencies 0.5, 0.78, 1, 1.2, 1.55, 1.9 THz and their corresponding absorption rates are 95, 85, 99, 87, 97 and 99% respectively. Even though silicon as a dielectric provides additional bands, its pressure resistance, temperature adaptability and mechanical stability are low and the absorption rates are less. The usage of polyimide as a substrate provides better tunable absorption bandwidth with a low cost when compared to Rogers RT 6010 as depicted in figure 6b. From table 1, it is inferred that the proposed absorber realises more number of absorption bands, size miniaturisation, frequency tuning with low complexity when compared with similar works that were reported earlier.

A perfectly designed absorber can act as a sensor that detects the optical signal and is hence suitable for placing in IoT backhaul networks. A metamaterial that acts as a strong resonant absorber at six different terahertz frequencies (0.5, 0.78, 1, 1.2, 1.55 and 1.9 THz) is reported. This absorber allows maximisation of the absorption spectrum by the independent tuning of every band by the potentially controllable graphene and also offers size miniaturisation up to $0.13\lambda_0 \times 0.13\lambda_0$. The absorptivity of more than 90% is obtained for most of the bands. This metamaterial is also a promising candidate as an absorbing element for temperature-based THz imaging, due to its relatively low volume, low density and multiband response. The following are the steps involved in processing a nominal metamaterial absorber:

Design process:

a) The cell structure was modelled and their electromagnetic characteristics were simulated by the commercial 3D electromagnetic simulator CST Studio Suite.

b) The automeshing technology and frequency-domain solver were used to acquire S-parameter.

c) The unit cell boundary condition with Floquet port was used to simulate the absorption spectra because the Floquet mode can be applied to any periodical array whether mirrored or rotated.

d) The resonance current distributions were obtained based on the field monitor technology of the CST at certain frequencies to determine its importance for resonance.

e) A numerical optimisation was performed through parametric simulation to obtain globally optimised design parameters of the said absorber element which includes physical length, width, height and patch dimension.

Table 1. Performance comparison with similar types of research works.

	This paper	[3]	[4]	[7]	[15]
No. of bands	6	1	1	2	1
BW coverage	0.3–2 THz	4.5–5.7 THz	2.24 THz	0.53–1.55 THz	180– 200 THz
Unit cell size	$0.13\lambda_0 \times 0.13\lambda_0$	$0.32\lambda_0 \times 0.32\lambda_0$	$0.27\lambda_0 \times 0.27\lambda_0$	$0.3\lambda_0 \times 0.3\lambda_0$	$5\lambda_0 \times 5\lambda_0$
Complexity	Low	Moderate	Low	Low	High
Tuning	Yes	Yes	No	No	Yes
Technique	Open ended stubs with graphene	Multilayer with photoresist	Capacitive golden layers	Array of patches	Multilayer with optical switch

f) An iterative optimisation process was performed to include all possible combinations of absorbing materials such as silicon, polyimide, etc.

g) The final design of the variables of the said absorbing element was selected from all possible combinations of optimised designs to approach the required design performance in the chosen frequency range

h) Thus, the thickness of the dielectric substrate (18 μm), its dielectric constant (3.5), the material used for the patch, i.e., Au, Ag, Cu, and the thickness of the ring (0.5 μm) were varied to obtain the desired operational frequencies.

Fabrication process:

Cu (thickness: 0.5 μm) was deposited on the silicon wafer by the sputtering process. Then, polyimide with 18 μm thickness was coated over Cu as a dielectric layer. Cu was deposited by the evaporation process. Finally, a metamaterial layer was formed by photolithography and wet etching process.

5. Conclusion

In this paper, a tunable hexaband absorber was proposed and validated for the frequency range of 0.1–2 THz. The effects of various conducting and dielectric materials on the absorption bands were analysed with the simulation results. The individual tuning of every absorption band by the respective L stubs graphene was well explained through the experimental graphs. The effect of current density on the absorption rate was verified with the surface current distribution diagram. With advanced technologies, it is feasible to have many emerging and future applications in the THz range in addition to the existing applications. Hence, the proposed absorber will play a vital role in the near future also.

References

[1] Zhihong Liu, Jiajia Liu, Yong Zeng and Jianfeng Ma, *IEEE Internet Things J.* **7**, 3378 (2020)

[2] Hang Yu, Bryan Ng and K G Winston, *IEEE Internet Things J.* **4**, 2217 (2017)

[3] Min Zhong, *IET Optoelectron.* **14**, 386 (2020)

[4] A Samy Saadeldin, Mohamed Farhat O Hameed and Essam M A Elkaramany, *IEEE Sens. J.* **19**, 7993 (2019)

[5] Rishi Mishra, Ravi Panwar and Dharmendra Singh, *IEEE Mag. Lett.* **9**, 1 (2018)

[6] Mohamad Nejat and Najmeh Nozhat, *IEEE Trans. Nanotechnol.* **18**, 684 (2019)

[7] Saeedeh Barzegar-Parizi and Amin Khavasi, *IEEE J. Quantum Electron.* **55**, 1 (2019)

[8] Mingyue Gu, Binggang Xiao and Sanshui Xiao, *Micro Nano Lett.* **13**, 631 (2018)

[9] Alireza Fardoost, Fatemeh Ghaedi Vanani and Amirhosseini, *IEEE Trans. Nanotechnol.* **16**, 68 (2017)

[10] Arya Fallahi and Alireza Yahaghi, *IEEE Trans. Antennas Propag.* **65**, 1464 (2017)

[11] Hong-En Su, Jia-Lin Li and Lei Xia, *IEEE Access* **18**, 161255 (2019)

[12] Yanfei Dong, Peiguo Liu, Dingwang Yu, Gaosheng Li and Liang Yang, *IEEE Antennas Wireless Propag. Lett.* **16**, 1115 (2017)

[13] Jing Yuan, Jun Luo and Ming Zhang, *IEEE Photon. J.* **10**, 1 (2018)

[14] Gang Yao, Furi Ling and Jin Yue, *IEEE Photon. J.* **1**, 1 (2016)

[15] Ferdows B Zarrabi, Maryam Bazgir and Reza Hekmati, *IEEE Photon. Technol. Lett.* **31**, 779 (2019)

[16] Yijia Huang, Jun Luo, Mingbo Pu and Yinghui Guo, *Adv. Sci.* **6**, 1801691 (2018)

[17] Xiangang Luo, *J. Phys. Photon.* **2**, 1 (2020)

[18] Lei Wang, Mengqiu Huang and Xuefeng Yu, *Nano-Micro Lett.* **12**, 1 (2020)